Analysis of Deployment and Inflation of Large Ribbon Parachutes

D. F. McVey* and D. F. Wolf†
Sandia Laboratories, Albuquerque, N. Mex.

A method for predicting deployment and inflation of reefed ribbon parachutes is presented. The method is based on integration of axial and radial momentum equations developed in the paper. Axial and radial forces are assumed to be describable by drag and radial force coefficients. Computer solutions of the equations are compared to measured parachute loads and to parachute mouth and maximum diameters from tests of 23- and 76-ft-diam conical ribbon parachutes. Comparison of load histories indicates that snatch loads depend to a large extent on deployment bag design and packing influences. Computed loads and parachute size histories for the inflation process compared favorably with flight data. The concept of a radial force coefficient appears to have considerable merit as a means of computing inflation for most types of parachutes.

Nomenclature

B = apparent mass coefficient
C_D = drag coefficient based on inflated diameter
C_R = radial force coefficient
D = drag, lb
e_c = ratio of minor axis to major axis for canopy equals 0.6 − constant
F = force, lb
g = acceleration of gravity, fps^2
L_i = arc length along inflated portion of canopy, ft
L_u = arc length along uninflated portion of canopy, ft
l = suspension line length, ft
m = mass, slug
m' = apparent mass, slug
M = total mass, slug
N = number of suspension lines
q = dynamic pressure, lb/ft^2
R = radial dimension, ft
S = reference area, ft^2
t = time, sec
T = tension, lb
T_{RL} = radial component of reefing line force, lb
V = velocity, fps
x = coordinate along flight path, ft
γ = flight path angle, below horizontal, deg
θ_c = inflated canopy half angle, deg
θ_l = one-half suspension line included angle, deg
θ_r = overinflation angle for reefed canopy, deg
λ_g = constructed geometric porosity, percent
λ_{gc} = geometric porosity corrected for canopy strain, percent
ϵ = strain
ρ = air density, slug/ft^3
ρ = density, slug/ft^3

Superscripts

$\cdot$ = first derivative with respect to time
$\cdot\cdot$ = second derivative with respect to time
$'$ = designates apparent mass

Subscripts

b = refers to parachute bag
c = refers to parachute canopy mass point
f = refers to forebody
l = parachute lines or linear
LS = line stretch
max = maximum valve
o = unstrained
p = refers to parachute
R = refers to radial direction
s = refers to parachute skirt mass point
x = refers to flight path direction

I. Introduction

IN general, adequate analytical methods have not been available to the parachute engineer for design and tradeoff studies. As a result, many parachute development programs have relied on expensive full-scale testing, i.e., design by testing. The work reported in this paper is part of a continuing program to develop analytical parachute design techniques that will permit reduction in the number of system field tests. Specifically, this paper discusses the development of mathematical models of deployment and inflation of ribbon parachutes. The analysis described considers the deployment sequence starting at first motion of the parachute bag through snatch load and inflation of an arbitrary number of reefed stages.

Heavy-duty ribbon parachutes have received considerable attention at Sandia Laboratories over the past 17 years.[1-3] These efforts have been primarily experimental; hence, a large quantity of full-scale flight test data for a wide range of parachute sizes and types are available. For comparison with the analytical methods, detailed information on deployment and inflation of a 23-ft-diam conical ribbon[2] parachute, and a 76-ft-diam concical ribbon[3] parachute was extracted from the available data. The 23-ft parachute contains 32 gores with a calculated geometric porosity of 23%. Continuous lengths of 9000-lb slotted webbing are used for the radials and 23.75-ft suspension lines. Continuous horizontal ribbons with reinforced selvage vary in strength from 3000 lb at the vent to 1000 lb at the skirt. A single stage of reefing is utilized. The 76-ft parachute contains 80 gores with a calculated geometric porosity of 16%. The 80-ft suspension lines are constructed of 3000-lb webbing, and three layers of 1500-lb 2-in.-wide ribbon are used for the radials. Horizontal ribbons vary in strength from 2000 lb at the vent to 460 lb at the skirt. The parachute was tested with both one and two stages of reefing. Although the results of the analysis

Presented as Paper 73-451 at the AIAA 4th Aerodynamic Deceleration Systems Conference, Palm Springs, California, May 21-23, 1973; submitted June 6, 1973; revision received November 29, 1973. This work was supported by the U.S. Atomic Energy Commission.

Index categories: Aircraft Deceleration Systems; Launch Vehicle Systems (Including Ground Support); Entry Deceleration Systems and Flight Mechanics (e.g., Parachutes).

*Supervisor, Deceleration and Recovery Systems Division. Member AIAA.

†Member of the Technical Staff, Deceleration and Recovery Systems Division. Member AIAA.

are compared with the flight data obtained from the two-ribbon parachutes, the methods are general and can be applied to a wide range of parachute systems.

The purpose of this paper is to present the development of the analytical methods and compare the mathematical models with flight test data.

II. Analysis

In the development of the governing equations, the parachute deployment sequence is broken into two phases. The first phase, which deals with deployment initiation through bag strip and continues until the parachute suspension lines and canopy are fully extended, includes the snatch load. The second phase begins with the parachute extended and includes the parachute inflation process.

In the solution procedure, the parachute is separated into finite mass elements which are connected to each other and to the vehicle by nonlinear springs. Mass fluxes are permitted between the mass elements as required by the deployment and inflation. Momentum equations are derived for the elements in directions parallel and normal‡ to the flight path. Time-rate of change of the momentum is then equated to the aerodynamic and gravitational forces acting on the parachute and vehicle. The resulting nonlinear, simultaneous, ordinary differential equations are solved on a digital computer.

Deployment and Bag Strip: Phase I

The system considered during deployment and bag strip is shown in Fig. 1. The assumptions applicable during this phase are as follows:

1) Lines are deployed first.

2) Drag of parachute bag and deploying lines are small compared to the drag of the pilot parachute.

3) The pilot parachute is fully inflated before deployment begins.

4) The apparent mass of air associated with the pilot parachute is negligible compared to the mass of the pilot and bag.

5) Time derivative of the apparent air mass is small in relation to the mass flux of the lines and canopy from the bag.

6) Both the vehicle and bag follow the same trajectory path.

7) The parachute radial momentum is negligible during Phase I.

Phase I Governing Equations—For the case of a control volume losing or gaining mass, the momentum equation (for one-dimensional motion) may be written[4]

$$\Sigma F = \frac{d}{dt}(MV) \pm \rho_l V_{abs} V_{rel} \tag{1a}$$

$$\Sigma F = M\frac{dV}{dt} + \frac{dM}{dt}(V \pm V_{abs}) \tag{1b}$$

where

+ is for the system losing mass

− is for the system gaining mass

MV = system momentum

V_{abs} = the absolute velocity of the mass added or removed from the system

V_{rel} = the velocity of the mass added or removed relative to the control volume.

A similar formulation of the momentum equation was used by Toni[5] to examine bag strip time; however, the snatch loading was not considered.

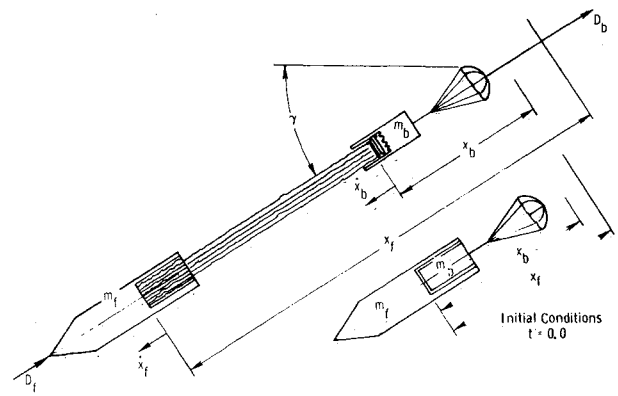

Fig. 1 System for snatch load computation.

Considering Fig. 1 and writing the mass of the forebody§ and bag as

$$M_f = m_f + \rho_l l_o \qquad M_b = m_b - \rho_l l_o$$

$$\dot{M}_f = \rho_l \dot{l}_o \qquad \dot{M}_b = -\rho_l \dot{l}_o$$

Equation (1a) may be written as

$$\Sigma F_f = m_f \ddot{x}_f \tag{2}$$

$$\Sigma F_b = m_b \ddot{x}_b + \rho_l \dot{l}_o(\dot{x}_f - \dot{x}_b) \tag{3}$$

Note that the elements of line mass are moving at a velocity $\dot{x}_f$ when they attach to the forebody.

By substituting the external forces associated with gravity, tension in the lines and aerodynamic drag into Eqs. (2) and (3) and by using the appropriate mass and mass flux equations

$$(m_f + \rho_l l_o)\ddot{x}_f = (m_f + \rho_l l_o)g \sin\gamma - \frac{\rho_\infty}{2}(C_D S)_f \dot{x}_f^2 - T \tag{4}$$

$$(m_b - \rho_l l_o)\ddot{x}_b = (m_b - \rho_l l_o)g \sin\gamma - \frac{\rho_\infty}{2}(C_D S)_b \dot{x}_b^2 + T - \rho_l \dot{l}_o(\dot{x}_f - \dot{x}_b) \tag{5}$$

Tension is obtained by solving for strain in the lines

$$\epsilon_l = ((x_f - x_b)/l_o) - 1 \tag{6}$$

and by obtaining the load [(P(ϵ)] from the load-strain diagram of the suspension line material. Tension is then

$$T = N[P(\epsilon)] \tag{7}$$

The line strip velocity $\dot{l}_o$ is obtained by equating the impulse applied to the lines to the change in momentum of the lines as they exit the bag. Referring to Fig. 3

$$\text{Impulse} = \Delta \text{ Momentum}$$

$$(T - F_l)\Delta t = \rho_l \Delta x_o(\dot{x}_f - \dot{x}_b)$$

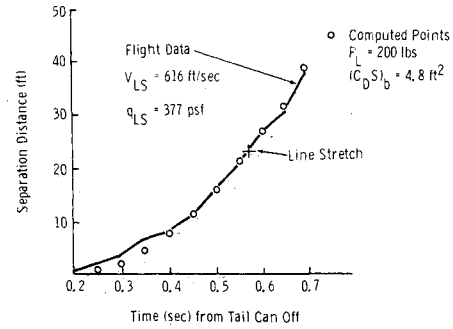

Fig. 2 Separation distance between forebody and bag, 23-ft parachute.

‡Normal direction corresponds to the parachute radial dimension.

§Forebody mass includes any portion of the lines and canopy that have been deployed from the bag.

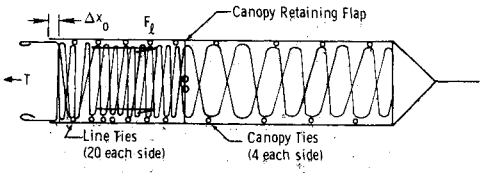

Fig. 3 Diagram of packed parachute.

where Δx_o is the unstretched length of line stripped in time Δt, and F_l represents internal bag forces caused by ties and/or friction

$$\lim_{\Delta t \to o} \frac{\Delta x_o}{\Delta t} = \dot{l}_o$$

and (8)

$$\dot{l}_o = ((T - F_l)/\rho_l(\dot{x}_f - \dot{x}_b))$$

Equations (4–8) along with the point mass ballistic trajectory equation for the flight path angle γ are solved on a digital computer. Input data include the load-strain curve for the suspension line material; the stretched-out parachute linear mass density distribution; pilot parachute drag, mass, and inflation time; vehicle mass and drag; and the initial trajectory conditions.

Snatch Load Data Comparison—Detailed comparisons of the bag strip and snatch loads were made for several full-scale tests of both the 23- and 76-ft-diam parachutes. The bag strip and time to full chute extension were matched accurately for both systems. A typical comparison is shown in Fig. 2. For the comparisons, the internal bag force was taken equal to 200 lb for the 23-ft parachute and 100 lb for the 76-ft parachute. The internal bag force results largely from breaking loops of nylon tape which tie the suspension lines to the bag and insure orderly deployment. The 23-ft pack contains 58 loops of 200-lb tape (breaking force ~400 lb), and the 76-ft pack contains 64 loops of 550-lb tape (breaking force ~1000 lb). Bag internal force was obtained by equating the total impulse required to break all the loops to the impulse of an average force F_l acting over the entire bag strip time. A sketch of a typical bag is shown in Fig. 3.

When computing snatch loads, it is usually assumed that the canopy acts as either a concentrated mass[11] or as a distributed mass[6] with some given linear density distribution as a function of canopy length. Initial calculations, assuming that the canopy acted as a concentrated mass throughout the snatch period, yielded loads 2 to 2.5 times greater than measured. Computed times to peak snatch load were also several times greater than observed. This led to the conclusion that the distributed mass assumption was most appropriate.

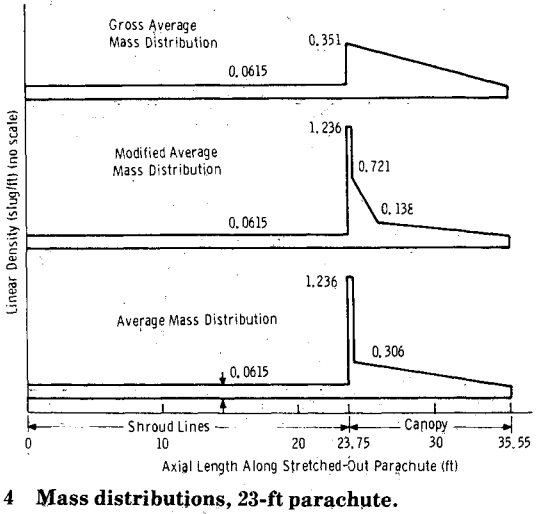

Fig. 4 Mass distributions, 23-ft parachute.

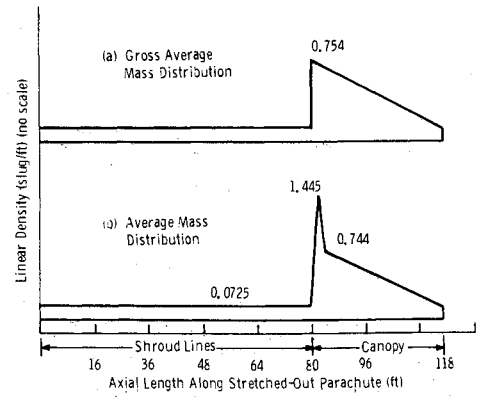

Fig. 5 Mass distributions, 76-ft parachute.

Load calculations were made for the mass distributions shown in Fig. 4 and 5 for the 23- and 76-ft-diam parachutes, respectively. The gross average mass distributions were obtained by assuming that the entire canopy mass (excluding radials) was distributed in a linearly decreasing manner over the length of the canopy. The average mass distributions were obtained by concentrating the mass of the skirt band, reefing line (or lines), reefing rings, and reefing line cutters in an appropriate width at the bottom of the canopy and distributing the remaining mass (excluding radials) over the remaining canopy length. The modified average distribution in Fig. 4 differs from the average distribution in that two-thirds of the canopy mass (excluding radials and the skirt mass) is arbitrarily assumed to be concentrated in the first 2 ft of the canopy length. A mass distribution of this type would result if, as a result of packing, the canopy tends to stick together during deployment.

The snatch load was found to depend strongly on two factors: 1) the time required for the canopy retaining flaps and bag lacings to react and release the canopy (after being cut) so that it can act as a distributed mass rather than a concentrated mass; and 2) the canopy mass distribution function, i.e., the manner in which the canopy is distributed and packed in the bag and how strongly it tends to stick together after the bag is cut. These factors are discussed in the following paragraphs.

Data from Maydew and Johnson[2] on peak snatch load as a function of dynamic pressure at line stretch are compared with computations in Fig. 6. The lower curve in the plot represents the computed snatch g as a function of dynamic pressure with distributed canopy and bag mass. This curve is valid for mass distribution, *b* or *c*, of Fig. 4. It is apparent that the curve lies below most of the data.

Several iterations with the computer code indicated that the only way the peak *g* of Fig. 6 and the load rise time could be matched was when the canopy and bag acted as a concentrated mass for a period of time. This time was determined in the following manner. It was hy-

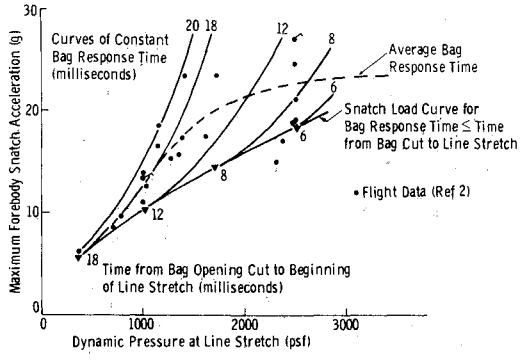

Fig. 6 Comparison of computed and measured snatch load variation with dynamic pressure, 23-ft parachute.

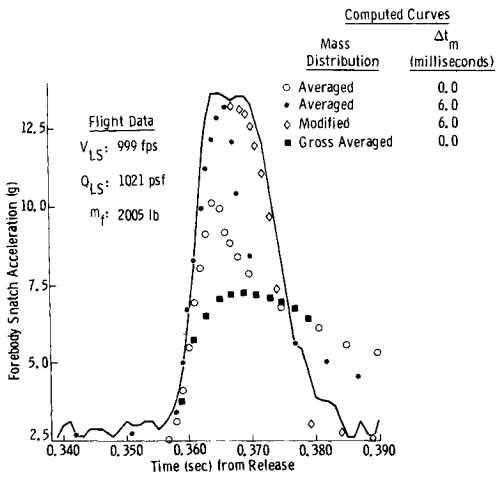

Fig. 7 Snatch load histories, test 352.

pothesized that a time interval would be required for the canopy retaining flaps and bag to relax sufficiently to release the canopy after being cut. This time interval was denoted as the "bag response time." In general, this time should decrease as dynamic pressure increases because the pressure acting on the inside of the bag forcing the lacing open would increase. Along with other factors, bag response time is also influenced by lacing load, pack density, and pack design. Curves for five bag response times are shown on Fig. 6. Four other times are also indicated along the lower curve in Fig. 6. These four times correspond to the interval (here called "cut delay") between the time the canopy retaining flaps are released by a cutter attached to the suspension line at 21.8 ft and the time at which the skirt extraction (line stretch) begins. Cut-delay time decreases as bag velocity and dynamic pressure increase. If, at a given dynamic pressure, the bag response time is less than the cut-delay time, the maximum snatch g will lie on the lower curve. If however, the bag response time is greater than the cut-delay time, the bag will act as a concentrated mass for an interval (Δt_m) equal to the difference in the two times. For example, at 2500 psf, the cut-delay time is about 0.006 sec. The two data points at about 19 g and 2500 psf are nearly on the 0.006-sec bag response time curve. For these points, the canopy and bag did not act as a concentrated mass. The flagged point at 27 g's lies on a bag response time curve of about 0.011 sec. Thus, the canopy and bag would act as a concentrated

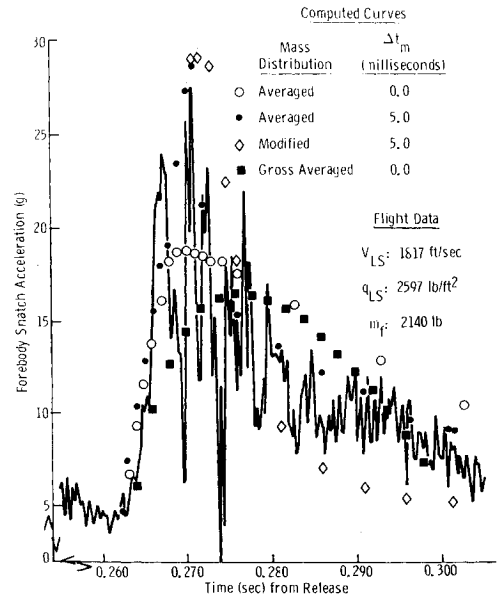

Fig. 8 Snatch load histories, test R-02.

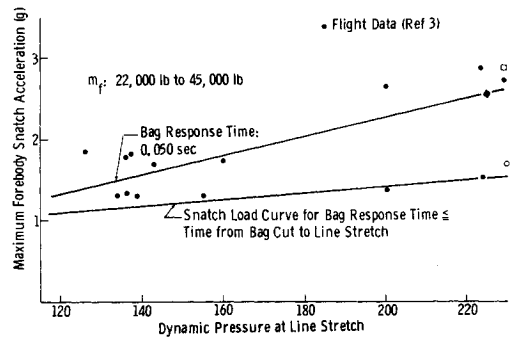

Fig. 9 Comparison of computed and measured snatch load variation with dynamic pressure, 76-ft parachute.

mass for $\Delta t_m = 0.011 - 0.006 = 0.005$ sec. In a similar manner, at 1000 psf, the g-level for the flagged point can be obtained by letting the bag and canopy act as a concentrated mass for $\Delta t_m = 0.018 - 0.012 = 0.006$ sec.

The most likely variation of bag response time for the 23-ft parachute pack configuration is shown by the dashed line on Fig. 6. This indicates that average bag response time decreases from about 0.020 sec at 300 psf to about 0.008 sec at 2500 psf. Note that the average bag response time curve would probably intersect the curve for bag response time less than bag cut time at about 3500 psf. At this point, the pressure force in the bag would probably release the bag immediately.

Timewise variations of snatch load for two of the tests analyzed are shown in Figs. 7 and 8. Load curves are shown for the case of bag response time less than bag cut time ($\Delta t_m = 0.0$) and for the appropriate Δt_m as interpreted from Fig. 6. It is noted that the curves for $\Delta t_m = 0.0$ tend to rise slower, peak lower, and have a longer decay than the measured data. The influence of altering the canopy mass distribution while keeping the skirt density constant is to alter the shape of the decay side of the g vs time curve. In general, comparison of the histories is reasonable. The modified average mass distribution seems to give better agreement at low dynamic pressure; on the other hand, the best agreement at high dynamic pressure would be obtained by the average distribution. As previously mentioned, the modified average attempts to account for the tendency of the nylon to stick together after being packed at high pressure. As would be expected, this tendency would be most apparent at low dynamic pressure. The result of ignoring the mass concentration at the skirt may be seen by comparing the snatch load history for the gross average mass curve with that of the average curve with the same Δt_m.

Comparison of measured and computed peak g versus dynamic pressure data for the 76-ft-diam parachute discussed by Holt[3] is given in Fig. 9. The mass distribution shown in Fig. 5b was used. Computed curves of peak snatch load for a bag response time of 0.050 sec and for the case of bag response time less than or equal to bag cut time are given. Bag cut time occurs when the canopy retaining flaps are released when 71 ft of the 80-ft suspension lines have been stripped from the bag. The 0.050-sec bag response time seems to represent a good average of the data. This is in reasonable agreement with the time that would be estimated from Fig. 6 for 150- to 250-psf dynamic pressure. It is noted that the percentage scatter in the 76-ft parachute snatch load data is somewhat greater than in the data for the 23-ft parachute; greater variation in packing may have caused the difference. Also intense interference from the B52 drop aircraft could be a factor in the scatter because the parachute is static line deployed near the aircraft. No data are available on snatch load histories for the 76-ft parachute.

The previous paragraphs have pointed out that observed variation in snatch loads could be explained in a consis-

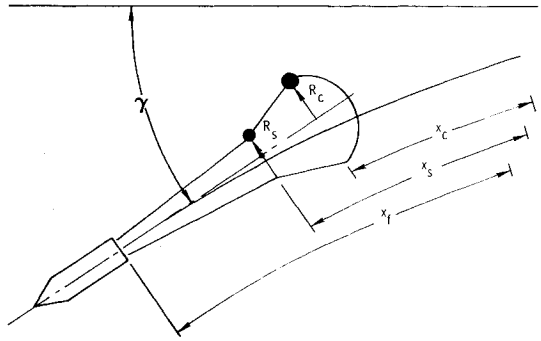

Fig. 10 Trajectory coordinates for inflation model.

tent manner by packing and bag influences as represented by a bag response time. Further work is under way to determine the parameters that influence the bag response time and to define methods of computing this important parameter. Until more complete data are available, it is probably reasonable to use bag response times of the magnitudes indicated by Fig. 6 for design with high-density (35–45 lb/ft^3) packs. It is also recommended that a linear mass distribution close to the actual be used in calculations when modeling deployment and snatch load histories.

Inflation: Phase II

The derivation of momentum equations which describe the motion of the forebody and parachute starting at line stretch and ending with the parachute fully inflated is discussed in this section. The method of analysis is an extension of a simpler model derived by Wolf,[7] which was based primarily on the earlier work of Weinig[8] and Toni.[9] The approach differs from methods developed by Heinrich[10] and others in that it utilizes momentum equations rather than a conservation-of-mass equation to describe the motion of the parachute canopy.

The major assumptions made for the inflation analysis are listed below:

1) The parachute canopy is modeled as two lumped masses, each with two degrees of freedom.

2) Aerodynamic forces are approximated by the sum of quasi-steady and fluid inertia forces.

3) Quasi-steady forces include a drag force proportional to parachute cross-sectional area and a radial force proportional to the inflated canopy area forward of the maximum radius point.

4) Fluid inertia forces proportional to axial and radial acceleration are included.

5) The portion of the canopy from the skirt to the maximum radius point is approximated by a conical frustum, while the canopy aft of the maximum radius is approximated by an oblate spheroid with constant eccentricity.

6) Elastic forces are obtained from static load-strain data for the materials used in the parachute.

7) The forebody and parachute are assumed to follow the same ballistic path.

Phase II: Governing Equations—The form of the momentum equation utilized is defined in Eq. (1b) for a system of variable mass. Trajectory coordinates used in the inflation model are defined in Fig. 10. Six degrees of freedom are required: three flight path coordinates (forebody, parachute skirt and parachute maximum radius point), two radial coordinates (parachute skirt and parachute maximum radius point), and the flight path angle.

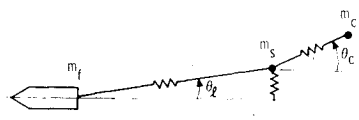

Fig. 11 Schematic of elastic components in inflation model.

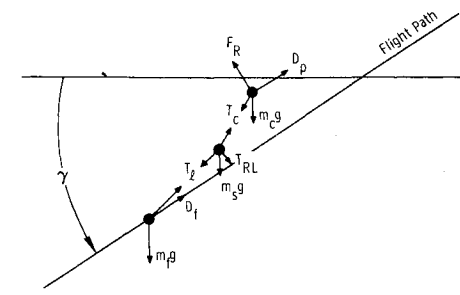

Fig. 12 System forces during inflation.

Masses representing the forebody, parachute skirt, and inflated parachute canopy are connected by elastic members as illustrated in Fig. 11. Forces on the respective masses are shown in Fig. 12. Canopy geometry is defined in Fig. 13.

Motion of the forebody along the flight path is described by Eq. (9)

$$m_f\ddot{x}_f = m_f g \sin\gamma - T_l \cos\theta_l - \frac{\rho_\infty}{2} C_{D_f} \dot{x}_f^2 S_f \qquad (9)$$

Rate of change of flight-path angle is obtained from the equation for conservation of momentum normal to the flight path, as in Eq. (10)

$$(m_f + m_p + m_{xc}')\dot{\gamma}\dot{x}_f = (m_f + m_p) g \cos\gamma \qquad (10)$$

All points on the axis of symmetry of the system are assumed to follow the same ballistic path.

Conservation of momentum [based on Eq. (1b)] for the mass concentrated at the parachute skirt is given by Eqs. (11) and (12):

$$m_s\ddot{x}_s = -T_c \cos\theta_c + T_l \cos\theta_l + m_s g \sin\gamma + \dot{m}_s(\dot{x}_c - \dot{x}_s) \qquad (11)$$

and

$$(m_s + m_{Rs}')\ddot{R}_s = T_c \sin\theta_c - T_l \sin\theta_l - T_{RL} + \dot{m}_s(\dot{R}_c - \dot{R}_s) - \dot{m}_{Rs}'\dot{R}_s \qquad (12)$$

Because the angle of the uninflated portion of the canopy is generally small, apparent mass or fluid inertia effects have been eliminated from Eq. (11). Forces required to accelerate mass from the skirt velocity to the canopy velocity are assumed to be provided at the skirt.

Similar momentum equations for the inflated canopy mass point are given by Eqs. (13) and (14):

$$(m_c + m_{xc}')\ddot{x}_c = T_c \cos\theta_c - \frac{\rho_\infty}{2} C_{Dc} S_c \dot{x}_c^2 + m_c g \sin\gamma - \dot{m}_{xc}'\dot{x}_c \qquad (13)$$

$$(m_c + m_{Rc}')\ddot{R}_c = -T_c \sin\theta_c - \dot{m}_{Rc}'\dot{R}_c + \frac{\rho_\infty}{2} C_R \dot{x}_c^2 (2S_c \sin\theta_c)\cos\theta_c \qquad (14)$$

In calculating the momentum flux effects associated with the apparent air mass terms, the simplifying assumption is made that the skirt and canopy exchange mass only with the surrounding air and not with each other. Reference area for the quasi-steady radial force is taken as the area of the inflated portion of the canopy forward of the point of maximum radius, or $2S_c \sin\theta_c$.

A simplified mass distribution for the parachute is assumed in the inflation analysis. This distribution is shown

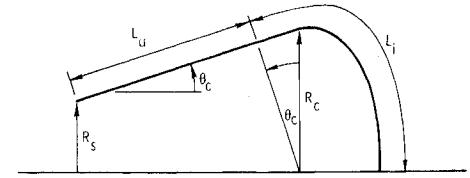

Fig. 13 Canopy geometry for inflation model.

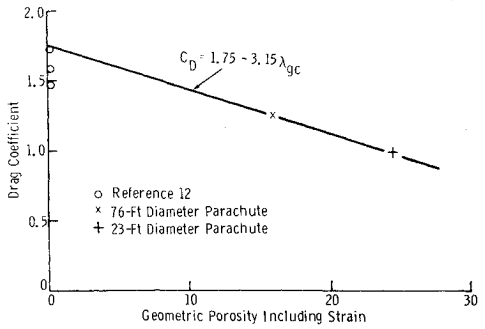

Fig. 14 Effect of porosity on full-open drag coefficient based on projected area.

in Fig. 4a for the 23-ft parachute and in Fig. 5a for the 76-ft parachute. Half the suspension line mass is assumed to be concentrated at the skirt, and the remaining half is assumed to be attached to the forebody.

Apparent mass terms in the equations of motion are expressed in the usual way as a coefficient times a characteristic mass of fluid

$$m_{xc}' = B_{xc}\rho_\infty(4/3)\pi R_c^3$$

$$m_{Rs}' = B_{Rs}\rho_\infty\pi R_s^2 L_u \cos\theta_c$$

$$m_{Rc}' = B_{Rc}\rho_\infty\pi R_c^3[(4/3)e_c + \sin\theta_c \cos\theta_c]$$

Mass flux terms are obtained by chain-rule differentiation. Although Ibrahim[11] has shown that geometric porosity has a significant influence on the magnitude of apparent mass coefficients, sufficient data do not exist to describe the porosity effect numerically. Therefore, estimates made in the simpler model[7] for numerical values of the mass coefficients are reduced here by a factor of two for the more porous ribbon parachutes. Numerical values used in this analysis are

$$B_{xc} = 0.25$$

$$B_{Rs} = B_{Rc} = 0.5$$

Examination of test data and films for the 23-ft and 76-ft parachutes indicated that the effects of porosity would have to be included in the quasi-steady force coefficients. In addition to the expected increase in drag with decreasing canopy porosity, an unexpectedly fast inflation was observed for the less porous 76-ft parachute. The faster inflation was most noticeable immediately after disreef. Based on test data for the two ribbon parachutes and a limited amount of wind tunnel data from Ref. 12, a highly simplified force coefficient model which includes geometric porosity effects was formulated. Also, because of the large unit strains (10 to 20%) which occur during the inflation of these parachutes, the coupled effect of strain on geometric porosity was estimated (for the dynamic model) from the relation

$$\lambda_{gc} = (\lambda_g + \epsilon_c)/(1.0 + \epsilon_c)$$

The linear variation of drag coefficient based on projected area with porosity shown in Fig. 14 was inferred from the data. Although the simple linear variation is not highly accurate over the entire porosity range, it at least

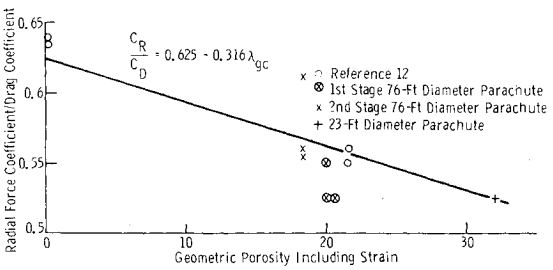

Fig. 15 Effect of porosity on radial force coefficient.

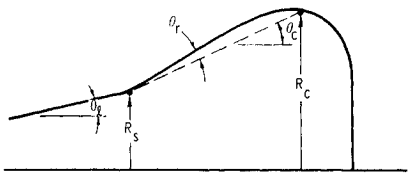

Fig. 16 Reefed parachute geometry defining overinflation angle.

provides a reasonable estimate of the level and slope of the curve in the region of interest for ribbon parachutes. Full open drag coefficient was used throughout the inflation.

A somewhat less straightforward, but still very simple, model of the radial force was formulated. During an equilibrium-reefed stage, the outward radial aerodynamic force must be in equilibrium with the inward component of the canopy elastic force. Equating these two force components for the steady-state condition results in the following approximate relation between radial force coefficient and drag coefficient

$$C_R/C_D = 1/(2\cos^2\theta_c)$$

On the basis of reefed-shape data taken from flight and wind-tunnel tests, the force coefficient ratio was inferred to vary with porosity as shown in Fig. 15.

In addition to the direct effect of porosity on radial force coefficient, a second porosity effect was included which was particularly noticeable at disreef. At disreef, the uninflated canopy for the very porous 23-ft parachute quickly becomes colinear with the suspension lines. This results in a reduction in the canopy inflated area and a slowing of the inflation after disreef. The angle of the uninflated canopy for the less porous 76-ft parachute always remains somewhat larger than the suspension line angle after disreef. A large acceleration and rapid inflation after disreef occur as a result. Although this complicated effect of porosity on canopy shape indicates that additional canopy degrees of freedom are probably required for a detailed description, a simple correction to the existing model was formulated, again on the basis of reefed-shape parachute data. The additional canopy angle appeared to be approximately equal to the reefed overinflation angle, θ_r (Fig. 16). The variation of θ_r with porosity for reefed parachutes was inferred to be linear, from the data shown in Fig. 17. Radial motion of the skirt and inflated canopy was constrained in the dynamic model so that $\theta_c \geq \theta_l + \theta_r$ throughout the inflation.

In order to provide starting conditions for numerical solutions to the equations of motion, initial values of skirt and canopy radius were taken from test data and all velocity components relative to the forebody were taken to be zero. Inflation is assumed to start at the skirt and proceed until the vent is inflated with no tension in the canopy. Once the vent region is inflated, elastic constraints are imposed throughout the remainder of the inflation.

Data Comparison—Solutions to the equations of motion were compared with available shape and load data for the 23-ft ribbon parachute and the 76-ft parachute. Shape and

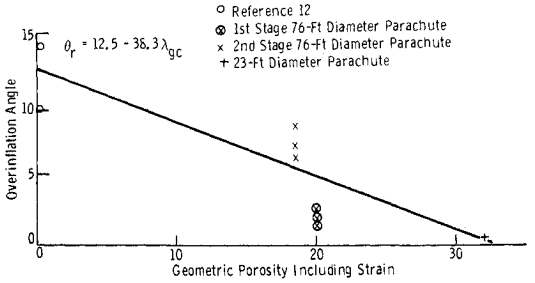

Fig. 17 Effect of porosity on reefed canopy angle.

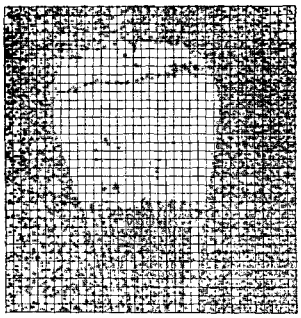

Fig. 18 Computer reading of parachute shape from test film, 23-ft parachute.

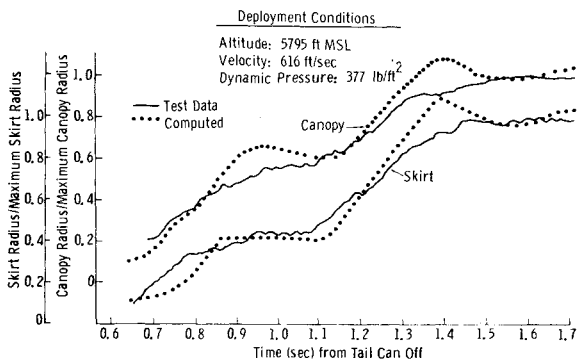

Fig. 19 Nondimensional radii vs. time, 23-ft parachute, test 359.

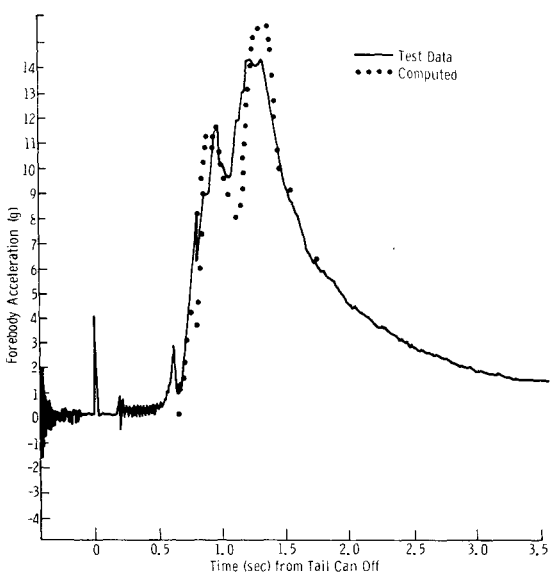

Fig. 20 Forebody acceleration data, 23-ft parachute, test 359.

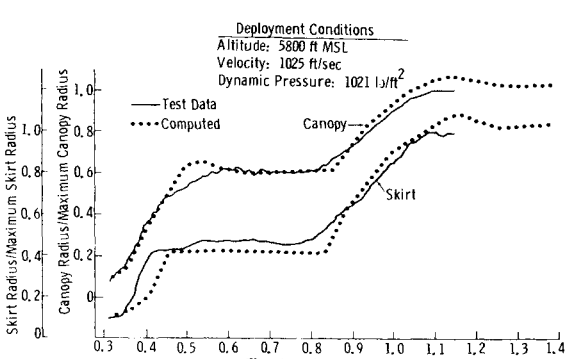

Fig. 21 Nondimensional radii vs. time, 23-ft parachute, test 352.

parachute dimensional data were obtained from computer-generated plots of digitized flight film frames, an

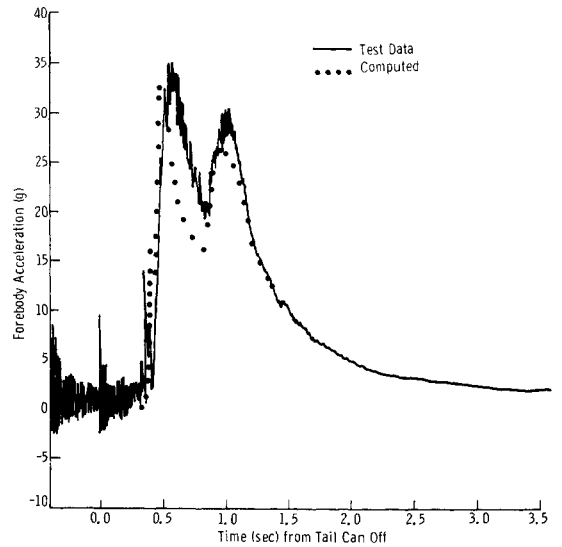

Fig. 22 Forebody acceleration data, 23-ft parachute, test 352.

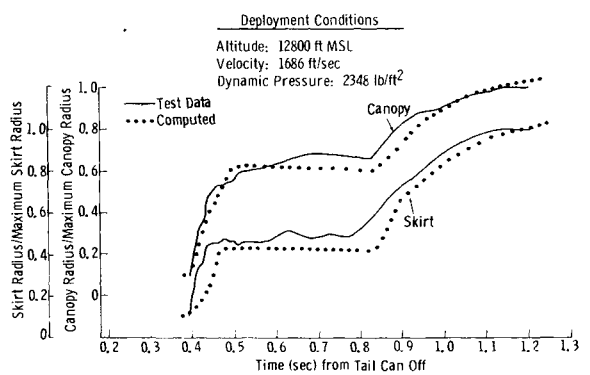

Fig. 23 Nondimensional radii vs. time, 23-ft parachute, test R-11.

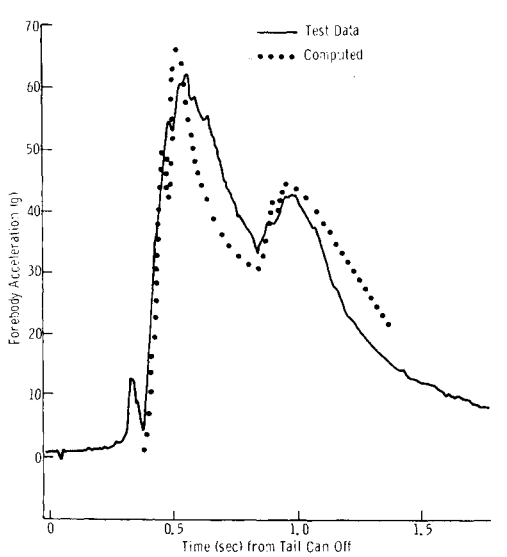

Fig. 24 Forebody acceleration data, 23-ft parachute, test R-11.

example of which is shown in Fig. 18. Force measurements were taken from forebody accelerometer data.

Comparisons of actual and predicted data for three tests of the 23-ft parachute are shown in Figs. 19–24. The data span the range of dynamic pressures over which the parachute was tested. The comparisons of predicted loads and shapes with the experimental data are good, considering the preliminary state of development and simplicity of the inflation model. The slight overinflation predicted by the dynamic model is probably caused by the absence of any

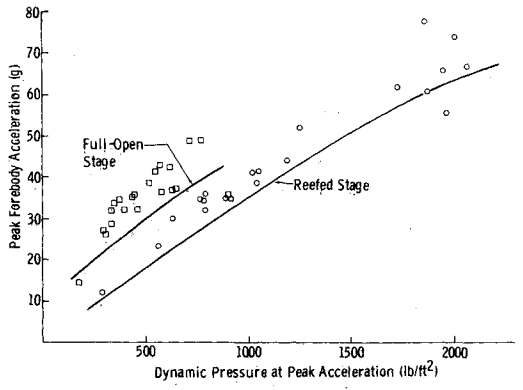

Fig. 25 Comparison of computed and experimental forebody acceleration data, 23-ft parachute, as a function of dynamic pressure.

canopy radial forces resulting from tension in horizontal ribbons. The rapid decrease in predicted force in the reefed stage suggests that the porosity correction to drag coefficient caused by canopy strain is probably excessive. A more realistic correction including the effective porosity concept of Heinrich[13] should improve the prediction. No serious attempts were made to "fine tune" the numerical solutions by adjusting the force and mass coefficients. Such "curve fitting" would seem pointless without additional independent calculation or measurement of these terms. Maximum force data in the reefed and full-open stages for a large number of tests of the 23-ft parachutes are compared with predicted forces in Fig. 25. Although the trends with dynamic pressure are good, the force levels are slightly low for both stages. An excessive drag coefficient correction associated with canopy strain is again the probable cause.

Data from a test of the 76-ft parachute are compared with predicted geometry and load data in Figs. 26 and 27. Again, some overinflation is predicted, although the steady shape is approximately correct. Because of the "double vent" construction of the 76-ft parachute,[3] the geometric porosity for the first stage of inflation is increased somewhat, but is not known accurately. Based on the data presented in Figs. 15 and 17, an estimated first-stage porosity of $\lambda_g = 20\%$ was used for the analysis. Also, the close proximity of the drop aircraft apparently caused a rather erratic first-stage inflation.

III. Conclusions

1) A dynamic model has been derived which predicts deployment and snatch loads. Variations in peak snatch loads for high-density parachute packs are explained in a consistent manner by bag influences as represented by a bag response time. Further work is needed to define the parameters that influence the bag response time and to define methods of computing this important parameter.

2) A dynamic inflation model has been derived which predicts reasonably well the variation of canopy shape and aerodynamic load with time for reefed ribbon parachutes.

3) Independent calculation and/or measurement of the force coefficients and apparent mass coefficients which appear in the equations of motion are required to improve the accuracy of the inflation model.

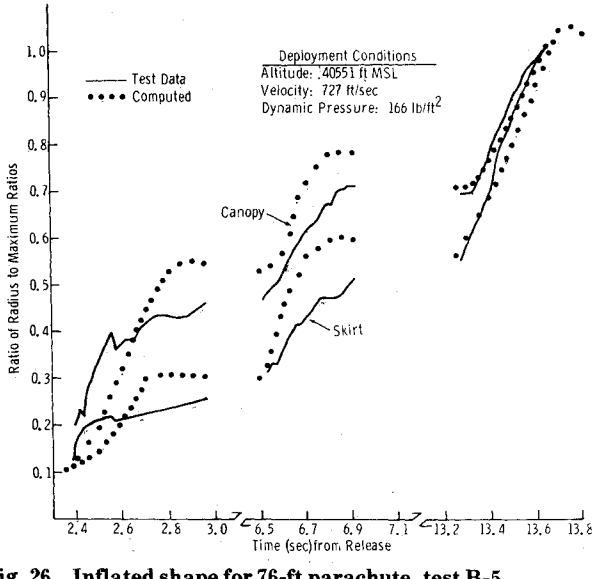

Fig. 26 Inflated shape for 76-ft parachute, test B-5.

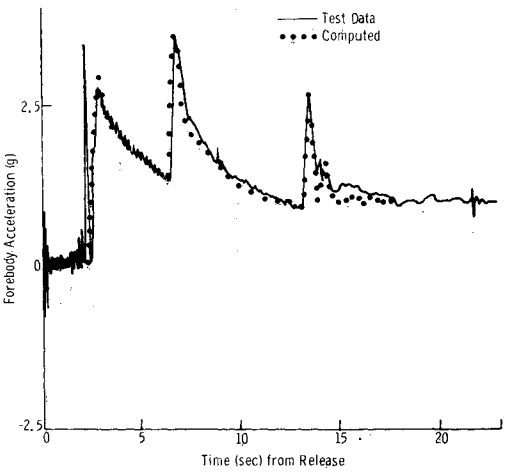

Fig. 27 Forebody acceleration data, 76-ft parachute, test B-5.

References

[1]Pepper, W. B., Jr. and Maydew, R. C., "Aerodynamic Decelerators—An Engineering Review," *Journal of Aircraft*, Vol. 8, No. 1, Jan. 1971, pp. 3-19.

[2]Maydew, R. C. and Johnson, D. W., "Supersonic and Transonic Deployment of Ribbon Parachutes at Low Altitudes," *Journal of Aircraft*, Vol. 9, No. 7, July 1972, pp. 497-502.

[3]Holt, I. T., "Design and Development of a Heavy Duty 76-ft Ribbon Parachute," *Proceedings Aerodynamic Deceleration Conference*, FTC TR 69-11, 1969, pp. 69-72.

[4]Greenwood, D. T., *Principles of Dynamics*, Prentice Hall, Englewood Cliffs, New Jersey, 1965, pp 165-168.

[5]Toni, R. A., "Theory on the Dynamics of Bag Strip for a Parachute Deployment Aided by a Pilot Chute," *Proceedings Aerodynamic Deceleration Conference*, FTC-TR-69-111, April 1969,

[6]Poole, L. R. and Huckins, E. K., "Evaluation of Massless-Spring Modeling of Suspension Line Elasticity During the Parachute Unfurling Process," NASA-TN-D-6671, Feb. 1972, NASA.

[7]Wolf, D. F., "A Simplified Dynamic Model of Parachute Inflation," AIAA Paper 73-450, Palm Springs, Calif., 1973.

[8]Weinig, F. S., "On the Dynamics of the Opening Shock of a Parachute," TR-6, Feb. 1951, USAF Office of Aeronautical Research, WADC, Dayton, Ohio.

[9]Toni, R. A., "Theory on the Dynamics of a Parachute System Undergoing its Inflation Process," AIAA Paper 70-1170, Dayton, Ohio, 1970.

[10]Heinrich, H. G., "A Linearized Theory of Parachute Opening Dynamics," *The Aeronautical Journal*, Vol. 76, No. 744, Dec. 1972, pp. 723-731.

[11]Ibrahim, S. K., "Experimental Determination of the Apparent Moment of Inertia of Parachutes," AFFDL-TDR-64-153, April 1965, Air Force Flight Dynamics Lab., Wright-Patterson Air Force Base, Ohio.

[12]Riffle, A. B., "Determination of the Aerodynamic Drag and Static Stability of Reefed Parachute Canopies," AFFDL-TR-64-166, Jan. 1965, Air Force Flight Dynamics Lab., Wright-Patterson Air Force Base, Ohio.

[13]Heinrich, H. G. and Greig, R. C., "Effective Porosity of Ribbon Grids," AFFDL-TR-65-110, Dec. 1965, Air Force Flight Dynamics Lab., Wright-Patterson Air Force Base, Ohio.